THE BELL SYSTEM TECHNICAL JOURNAL
Vol. 59, No. 7, September 1980
Printed in U.S.A.

A Polynomial Model for Multipath Fading Channel Responses

By L. J. GREENSTEIN and B. A. CZEKAJ

(Manuscript received January 10, 1980)

We present a channel model useful for analyzing the effects of multipath fading in digital radio systems. The frequency response of a fading channel is represented by the function $A_0 - \omega B_1 + j\omega A_1$, *where* ω $(=2\pi f)$ *is measured from the center of the channel, and* A_0, A_1, *and* B_1 *are variable coefficients that change slowly with time. The model consists of this function, the joint probability density function (pdf) for the three coefficients, and the average number of seconds per heavy-fading month for which this response applies. The model is derived from a large base of multipath fading data, obtained on a 26.4-mile path in Georgia in June 1977. It consists of nearly 25,000 recorded measurements of received power vs frequency in a 25.3-MHz bandwidth at 6 GHz. In this paper, we present the methods of data reduction and statistical analysis used to derive the model; describe some assessments of its validity; and discuss its limitations, virtues and possible uses. By all available measures, the model is highly accurate. It suffers from a potentially important phase ambiguity that can be resolved only via new, coherent measurements. The existing model should prove very useful in the design and planning of such measurements.*

I. INTRODUCTION

Multipath fading in microwave digital radio systems can be a major source of outage and, therefore, has been the subject of numerous recent investigations.[1-4] One important objective of current activity is to develop a statistical model of fading useful for estimating its effect on specific systems and for indicating possible methods of correction.

Two multipath fading characterizations have been proposed recently for terrestrial systems in the channelized common carrier bands. One represents the multipath fading frequency response as that due to an equivalent three-path medium.[5] The result is a three-parameter, com-

plex gain function, where the joint probability distribution for the three parameters describes the fading statistically. The second characterization, which is the subject of this paper, expresses the multipath fading frequency response as a complex polynomial expanded about the channel center frequency.[6] Specifically, if

$$H_c(\omega) \triangleq \frac{\text{complex channel gain at any time}}{\text{complex channel gain during nonfading}}, \tag{1}$$

where $\omega(=2\pi f)$ is measured from the center frequency, then the polynomial representation is

$$H_c(\omega) = A_0 + \sum_{n=1}^{N} (A_n + jB_n)(j\omega)^n, \tag{2}$$

where the A- and B-coefficients vary slowly relative to the speeds of typical digital radio systems.

Note that $H_c(0)$ is just A_0, a real number, i.e., we arbitrarily (and with no loss in generality) specify the phase shift at the channel center frequency to be zero.

The polynomial function of eq. (2) can fit frequency responses of any shape with arbitrary accuracy merely by choosing N sufficiently large. Moreover, the difficulty of fitting coherently measured responses does not grow significantly with N since $H_c(\omega)$ is linearly related to the characterizing parameters (the A_n's and B_n's).

Several features make the polynomial representation attractive for multipath modeling. One is that it leads to simple methods for analyzing signal processing (note that $(j\omega)^n$ corresponds to the nth time derivative). A second is that it suggests a promising idea for adaptive equalization; specifically, the rational function $1/H_c(\omega)$ may be easy to realize adaptively when the complex zeros of $H_c(\omega)$, (2), have negative real parts. A third feature is parsimony, suggested by the conjecture[6] that a first-order function ($N = 1$) may be sufficiently accurate for terrestrial paths in the channelized bands below 15 GHz. In that case, the channel response function could be characterized by three linear coefficients (A_0, A_1, and B_1).

The work reported here has confirmed this conjecture for the data base used by Rummler.[5] The central activity has been to compute A_0, A_1, and B_1 from the recorded measurements and to analyze their joint statistics. The outcome is a model for the joint pdf, $p(A_0, A_1, B_1)$, that can be used to assess multipath effects in any digital radio system.

Section III presents a mathematical description of the new model. Section II gives an overview of the data reductions and analyses leading to this model, while Section IV gives an expanded discussion for readers interested in more details.

Section V discusses the accuracy of the derived model and presents supporting evidence for the steps taken to simplify it. Part of this

evidence is obtained by calculating outage times for numerous system approaches, using model versions of differing complexity. This exercise not only validates the simplest version but illustrates its important application to system studies. Section VI summarizes the uses and limitations of the model and cites the need for further measurements to reinforce and improve it.

II. DATA REDUCTIONS

2.1 The data base

The multipath fading data base is a set of measurements made on a 26.4-mile path in Palmetto, Georgia in June 1977.[5] During fading events, received power was measured at each of 24 frequencies distributed about 6034.2 MHz and spaced by 1.1 MHz. The measuring filter at each frequency had a 200-KHz bandwidth. The power samples were normalized by the unfaded received power level (as estimated from mid-day measurements), converted to decibels, quantized in 1-dB steps, and recorded on magnetic tape. Because of an equipment failure, data for the 19th frequency in the sequence (7.15 MHz above the center of the channel) were not obtained.

Each tape record therefore consists of 23 power response values, in quantized decibels, corresponding to a single measurement. No phase response data were recorded, resulting in unresolvable ambiguities in the reductions, as discussed later. Measurements were recorded at rates of either five per second or one per two seconds, depending on the speed of change in the fading response. The data base used here consists of 24,920 records spanning, roughly, 8400 seconds of fading.

2.2 The polynomial coefficients

The main reductions consist of (i) determining the coefficients in eq. (2) for each record in the data base and (ii) finding a mathematical description of the joint probability density function (pdf) of these coefficients. In this subsection, we outline the strategy used for determining the coefficients.

Each data record consists of the quantized values of $-10 \log_{10} |H_c|^2$ at 23 frequencies, where H_c is the complex channel gain.

We denote the recorded values by the set $\{P_i\}$, where i is the frequency index ($i = 1, 24$ excluding 19). The data reduction per record begins by converting each decibel quantity P_i into a power ratio $p_i (= 10^{-P_i/10})$, and fitting the sequence of p_i vs frequency with an Mth-order polynomial,

$$q(\omega) = D_0 + \omega D_1 + \cdots \omega^m D_m + \cdots \omega^M D_M. \tag{3}$$

In obtaining the coefficients ($D_0, \cdots D_M$), a form of least-squares optimization has been used, and M-values of 0, 2, and 4 have been

tried. We have evaluated the errors between the p_i's and the fitting function $q(\omega)$ for each record and have studied the statistics of these errors over the ensemble of records that comprise the data base. Our finding is that, given the noise statistics and bandwidth of the measurements, the most suitable polynomial order is $M = 2$. For, when $M = 0$, the fitting function lacks the curvature needed to model the true fading response, while, when $M = 4$, the third- and fourth-order polynomial terms serve more to fit the measurement noise than to fit the underlying response. The curvature provided by $q(\omega)$ when $M = 2$ seems to be just right for the 25.3-MHz measurement bandwidth. For that case, we estimate the rms fractional difference between $q(\omega)$ and the true power response to be 5 percent at all frequencies.

Given a value for M and a procedure for obtaining the D_m's from the data records, we must choose the order (N) of the polynomial in eq. (2) and derive the A_n's and B_n's in that equation from the D_m's. Before deciding on N, we note that a power-gain function can be obtained from eq. (2) having the form

$$|H_c(\omega)|^2 = \hat{D}_0 + \omega\hat{D}_1 + \cdots \omega^m\hat{D}_m + \cdots \omega^{2N}\hat{D}_{2N} \tag{4}$$

where the $\hat{D}_m$'s are simply related to the A_n's and B_n's. The objective is to match this function to $q(\omega)$ in eq. (3).

One possibility is to choose $N = M/2$ and to find the A_n's and B_n's for which $\hat{D}_0 = D_0$, $\hat{D}_1 = D_1$, etc. The problem is that, if D_M happens to be negative, this important term cannot be matched using all real A_n's and B_n's. The approach we have used instead is to specify $N = M$, and to choose the $(2N + 1)$ A_n's and B_n's so that

$$\hat{D}_m = \begin{cases} D_m; & 0 \le m \le N \\ 0; & N < m \le 2N. \end{cases} \tag{5}$$

This procedure, however, is limited in at least one and sometimes two respects. The fundamental limitation concerns those A_n's and B_n's contained within the imaginary part of $H_c(\omega)$, *i.e.*, (A_1, A_3 $\cdots$ B_2, B_4 $\cdots$). Given a valid solution to eq. (5), reversing all these coefficients in sign results in exactly the same function for $|H_c(\omega)|^2$. Thus, there are two possible solutions, each of which is equally valid given the data.

The polarity ambiguity in the subset (A_1, A_3, $\cdots$ B_2, B_4 $\cdots$) is reflected as a polarity ambiguity in the phase response associated with $H_c(\omega)$, an inevitable consequence of noncoherent measurements. Our reduction approach is to assume equally likely polarities for any given fade. In computing A_n's and B_n's for each record, we have randomly selected the polarity in accordance with this assumption.

A second limitation on the application of eq. (5) arises when the $\hat{D}_m$'s for $n > N$ cannot all be forced to zero using real A_n's and B_n's. In performing reductions for $N = 2$, for example, a solution with real A_n's and B_n's is only possible when

$$\Delta = (D_2 - D_1^2/4D_0) \geq 0. \tag{6}$$

We will limit all remaining discussions to the case $N = M = 2$.

The condition $\Delta \geq 0$ corresponds roughly to $q(\omega)$ being concave over the measurement bandwidth. In such cases, $A_2 = B_2 = 0$, and the function for $H_c(\omega)$ reduces to a first-order polynomial. When $\Delta < 0$ ($q(\omega)$ more or less convex over the measurement bandwidth), no real combination of A_n's and B_n's will satisfy all of eq. (5). This condition is found to occur over 42 percent of the data base. Our strategy for these cases is to choose $(A_0, A_1, A_2, B_1, B_2)$ so that $(\hat{D}_0, \hat{D}_1, \hat{D}_2)$ matches (D_0, D_1, D_2); $\hat{D}_3 = 0$; and $\hat{D}_4 (= A_2^2 + B_2^2)$ has the smallest magnitude possible for real A_n's and B_n's. The result is a fourth-order component in $|H_c(\omega)|^2$, namely, $\omega^4 \hat{D}_4$, which we have found to be relatively small (in a sense that we define later).

The above strategy leads to the following set of solutions:

$$A_0 = \sqrt{D_0}; \tag{7a}$$

$$B_1 = -D_1/2A_0; \tag{7b}$$

$$A_1 = \begin{cases} \pm\sqrt{\Delta}; & \Delta \geq 0 \\ \pm\dfrac{1}{2}\sqrt{-B_1^2 + B_1\sqrt{B_1^2 - 8\Delta}}; & \Delta < 0 \end{cases} \tag{7c}$$

$$A_2 = \begin{cases} 0; & \Delta \geq 0 \\ \dfrac{A_1^2}{A_0}\left(1 + \dfrac{A_1^2}{B_1^2}\right); & \Delta < 0 \end{cases} \tag{7d}$$

and

$$B_2 = A_2 B_1 / A_1. \tag{7e}$$

In computing these coefficients, the polarity of A_1 is chosen randomly for each record.

The question arises of how the model should take account of the two distinct conditions on Δ. One idea is to treat all computed combinations of (A_0, A_1, B_1) as part of a single statistical population, without differentiating between the conditions $\Delta \geq 0$ and $\Delta < 0$, and to assume that $A_2 = B_2 = 0$ in *all* cases. The result would be a first-order polynomial for $H_c(\omega)$ defined by a single joint pdf of A_0, A_1 and B_1. This approach has been adopted for reasons of modeling simplicity, and is justified by data given in Section V.

2.3 The coefficient statistics

We begin the statistical modeling with the coefficient A_0, representing the complex channel gain at $\omega = 0$. The probability distribution of

A_0 is found to be approximately log-normal, i.e., if

$$ADB \triangleq 20 \log_{10} A_0, \tag{8}$$

then the pdf of ADB is approximately Gaussian, with a mean (μ) of -21.39 dB and a standard deviation (Σ) of 6.562 dB. For convenience, we shall deal with ADB in terms of the standardized variable

$$a_o \triangleq (ADB - \mu)/\Sigma. \tag{9}$$

The precise pdf for a_o used in the model is presented in Section III.

The joint probability law for A_0, A_1, and B_1 can be represented by the joint pdf of A_1 and B_1, conditioned on a_o, times the pdf of a_o. Furthermore, system study results (Section V) indicate that A_1 and B_1, for given a_o, can be modeled as independent variables. Hence, we write

$$p(A_1, B_1 \mid a_o) = p_A(A_1 \mid a_o) p_B(B_1 \mid a_o). \tag{10}$$

To model $p_A(\,|\,)$ and $p_B(\,|\,)$, the entire population of data records was divided into 11 subpopulations, each corresponding to a specific interval of a_o. For example, all records with a_o between -2.25 and -1.75 constituted one such subpopulation, all those with a_o between -1.75 and -1.25 constituted another, and so on. Within each subpopulation, we computed the mean and standard deviation of A_1, as well as its probability distribution, and similarly for B_1.*

Both A_1 and B_1 are found to be essentially Gaussian in every subpopulation; in every case, moreover, each variable has a zero mean and a standard deviation that varies with the mid-value of a_o. Consequently, the joint pdf of A_1 and B_1, conditioned on a_o, reduces to a product of two Gaussian pdf's, each with a standard deviation that is a function of a_o. By finding suitable mathematical expressions for these functions, the statistical modeling of A_0, A_1, and B_1 is completed.

A final quantity to determine is the number of seconds, T_M, for which the multipath fading response applies in a heavy-fading month. The data base used here represents about 8400 seconds of fading which, Lundgren and Rummler have estimated, corresponds to two-thirds of a heavy-fading month for the measured path and frequency.[4] In attempting to relate this finding to other paths and frequencies, we have assumed that T_M is proportional to the multipath occurrence factor developed by Barnett.[7] This assumption permits the general expression for T_M given in the following section.

---

* The choice of 11 subpopulations and the particular a_o-intervals used is somewhat arbitrary. Our aim was to obtain both good resolution (narrow intervals of a_o) and high estimation accuracy (many samples per subpopulation).

III. THE MODEL

In this description, all numerical quantities in braces, { }, are data-derived constants that may vary with path length, antennas, locale, year, etc. It is hoped that the underlying model *structure*, consisting of the form of the transfer function and the functions for the coefficient pdf's, is generally applicable and that the constants alone might be subject to change. In any event, what follows is an estimated fading model based on reductions of the given data.

(*i*) The complex transfer function of a channel, normalized by its unfaded gain, is

$$H_c(\omega) = \begin{cases} 1 + j0 & \text{during non-fading periods;} \\ A_0 - \omega B_1 + j\omega A_1 & \text{during } T_M \text{ seconds per heavy-fading month.} \end{cases} \tag{11}$$

(*ii*) By assuming T_M to be proportional to the multipath occurrence factor,[7] we obtain

$$T_M = \{0.11\}\, cFd^3, \tag{12}$$

where c is the terrain factor, F is the system frequency in gigahertz, and d is the path length in miles.

(*iii*) The joint pdf of A_0, A_1, and B_1 (where A_0 is dimensionless and A_1 and B_1 are in units of seconds) can be represented by

$$p(a_o, A_1, B_1) = p_A(A_1 \mid a_o) p_B(B_1 \mid a_o) p_a(a_o), \tag{13}$$

where

$$a_o = \frac{20 \log_{10} A_o - \{-21.39\}}{\{6.562\}}. \tag{14}$$

(*iv*) The pdf of a_o is the nearly Gaussian function

$$p_a(a_o) = \frac{1}{\sqrt{2\pi}} \exp\left[-\frac{1}{2}[a_o + z(a_o)]^2 \right] \cdot \left[1 + \frac{dz(a_o)}{da_o} \right], \tag{15}$$

where $z(a_o)$ is a small nonlinear term in a_o given by

$$z(a_o) = \{0.0742\} a_o^2 + \{0.0125\} a_o^3. \tag{16}$$

If this component were zero, $p_a(a_o)$ would be precisely Gaussian. Figure 1a shows $p_a(a_o)$ and compares it with the Gaussian pdf having the same mean (0.0) and variance (1.0). The difference seems small but has been found to be significant, as we will discuss in Section 5.2.

(*v*) The conditional pdf's of A_1 and B_1, $p_A(A_1 \mid a_o)$ and $p_B(B_1 \mid a_o)$, are both Gaussian with zero means and with standard deviations given by

$$\sigma_A = \text{Max}\{\{0.14\}, [\{0.309\} + \{0.13\} a_o]\} \times 10^{-9} \text{ s} \tag{17}$$

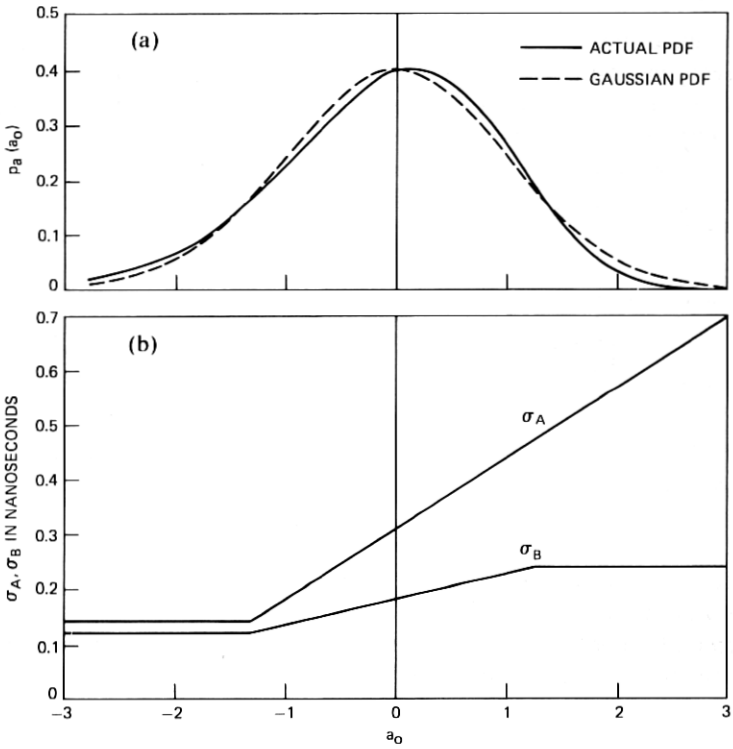

Fig. 1—Functions used in the multipath fading model: (a) the pdf of a_o, compared with a normal (Gaussian) pdf; and (b) the standard deviations of A_1 and B_1, conditioned on a_o.

and

$$\sigma_B = \text{Min}\{\{0.24\}, \text{Max}(\{0.12\}, [\{0.18\} + \{0.046\}a_o])\} \times 10^{-9} \text{ s.} \quad (18)$$

These functions, which model the variations of σ_A and σ_B with a_o, are shown graphically in Fig. 1b. They are derived by estimating σ_A and σ_B from finite numbers of records in nine a_o-intervals of finite width. The results are therefore quite approximate; our tests indicate, however, that they are not sensitive to the precise positions or widths of the a_o-intervals.

IV. DATA REDUCTIONS: EXPANDED DISCUSSION

This section presents mathematical, numerical, and graphical details underlying the data reductions and the construction of the model. The interested reader can thereby scrutinize the various stages of analysis and reasoning that led to the results in Section III. The less interested reader can, with no loss in continuity, proceed to Section V.

4.1 Data organization and notation used

The data base consisted originally of 24,920 records of decibel power gain vs frequency. An early decision was made to remove the first 100 records in the sequence, as they contained a number of normal (non-fading) responses. The model is derived from the resulting set of 24,820 records.

The second decision made was to create four subsets of data records, each containing about 2160 records distributed randomly over the total set (24,820 records). The aim was to verify the statistical regularity of the data base, i.e., to establish that no handful of records dominates the statistics and that individual subsets are representative of the data base as a whole. Having verified this regularity (by comparing results among the four subsets and between the four subsets and the total set), we were able to perform certain costly reductions using a relatively small set of records.

All computations in this study were performed using, as a data base, either the four individual subsets, the four subsets merged together (8640 records), or the total set of 24,820 records. In every case, we have found it helpful to regard the prevailing data base as an *ensemble* of records, each record being a sequence of 23 power gains. The notations, symbols, and definitions used in all computations are summarized in Table I, which should be consulted throughout subsequent discussions.

4.2 Deriving the polynomial coefficients

The process begins with 24,820 records of P_i vs i and ends with a population of coefficient sets, (A_0, A_1, B_1), whose reduction to a joint probability law (Sections III and 4.3) defines the fading model. Three stages of computation are involved here, namely, (*i*) adjusting the recorded P_i's to remove systematic calibration differences across the 23 measurement frequencies, (*ii*) determining, from these adjusted data, the optimal polynomial order and the resulting record-by-record coefficients of the power gain function, eq. (3), and (*iii*) determining, from these coefficients, the record-by-record coefficients of the complex gain function, eq. (2). We now discuss these three stages in turn.

4.2.1 Data adjustments

From physical considerations, we would expect the ensemble probability law for P_i to be the same for all i. Thus, the power gain at any given frequency should exhibit the same statistical behavior as that at any other frequency. This expectation is confirmed by the data, which show that the probability law for P_i is approximately Gaussian for all i. At the same time, however, the data show small but discernible variations of $\bar{P}_i$ and σ_i with i.

Table I—Symbols and Definitions

Symbol	Definition
i	Index of frequency ($i = 1$ for lowest frequency; $i = 24$ for highest frequency).
$\bar{x}_i$	Average of x_i over ensemble of records comprising data base (x_i can be any variable).
$\langle x_i \rangle$	Average of x_i over i for given record; $\langle x_i \rangle = \frac{1}{23} \sum_{\substack{i=1 \\ \neq 19}}^{24} x_i.$
R_i	Actual channel power gain, in dB, at ith frequency.
P_i	Recorded channel power gain, in dB, at ith frequency.
p_i	Power gain ratio at ith frequency; $p_i = 10^{P_i/10}$.
$q(\omega)$	Polynomial fitted to sequence of p_i's; $q(\omega) = \sum_{m=0}^{M} D_m \omega^m$.
Q_i	Decibel value of $q(\omega)$ at ith frequency (represents fitted approximation to P_i); $Q_i = 10 \log q(\omega_i) \equiv 10 \log q_i$.
σ_i^2	Ensemble variance of P_i; $\sigma_i^2 = \overline{P_i^2} - (\overline{P_i})^2$.
e_i	Measurement error, $(P_i - R_i)$, at ith frequency; $\overline{e_i^2} = \sigma_{\text{meas}}^2$, all i.
E_i	Observed error, $(P_i - Q_i)$, at ith frequency.
ϵ_i	Modeling error, $(Q_i - R_i)$, at ith frequency.
E_{rms}^2	Mean-square observed error per record; $E_{\text{rms}}^2 = \langle E_i^2 \rangle$.
$\hat{E}_{\text{rms}}^2$	Approximation to E_{rms}^2 (quadratic in q_i); $\hat{E}_{\text{rms}}^2 = \left\langle \left\{ \frac{10}{\ln 10} \frac{p_i - q_i}{p_i} \right\} \right\rangle^2.$
E_B	Bias in observed errors per record; $E_B = \langle E_i \rangle$
$E_i^{(k)}$	kth root of kth central moment of E_i over ensemble; $E_i^{(k)} = \sqrt[k]{\overline{(E_i - \bar{E}_i)^k}}$.

These variations were computed for the total record set and for each of the four record subsets. Results are given in Fig. 2, where the vertical bars span values for the four subsets and the solid curves connect the values for the total set. Also given are results for the decibel value of $\bar{p}_i$. The variations for this quantity are virtually parallel to those for $\bar{P}_i$, a consequence of the fact that the pdf of P_i has roughly the same shape and variance for every i.

For all three quantities ($\bar{P}_i$, σ_i and $\bar{p}_i$), the consistency of results is evident among the four subsets and between those subsets and the total set. For each quantity, moreover, the average variation with i is more pronounced than the spread among the data subsets. These findings make clear that the variations with i are not statistical but, rather, the result of systematic calibration differences in the measurements. The variations with i of $\bar{P}_i$, in particular, can be explained in terms of such systematic differences. Comparable explanations for the variations of σ_i are not as forthcoming. Nevertheless, a decision was made to attribute the nonuniformities of both $\bar{P}_i$ and σ_i to systematic

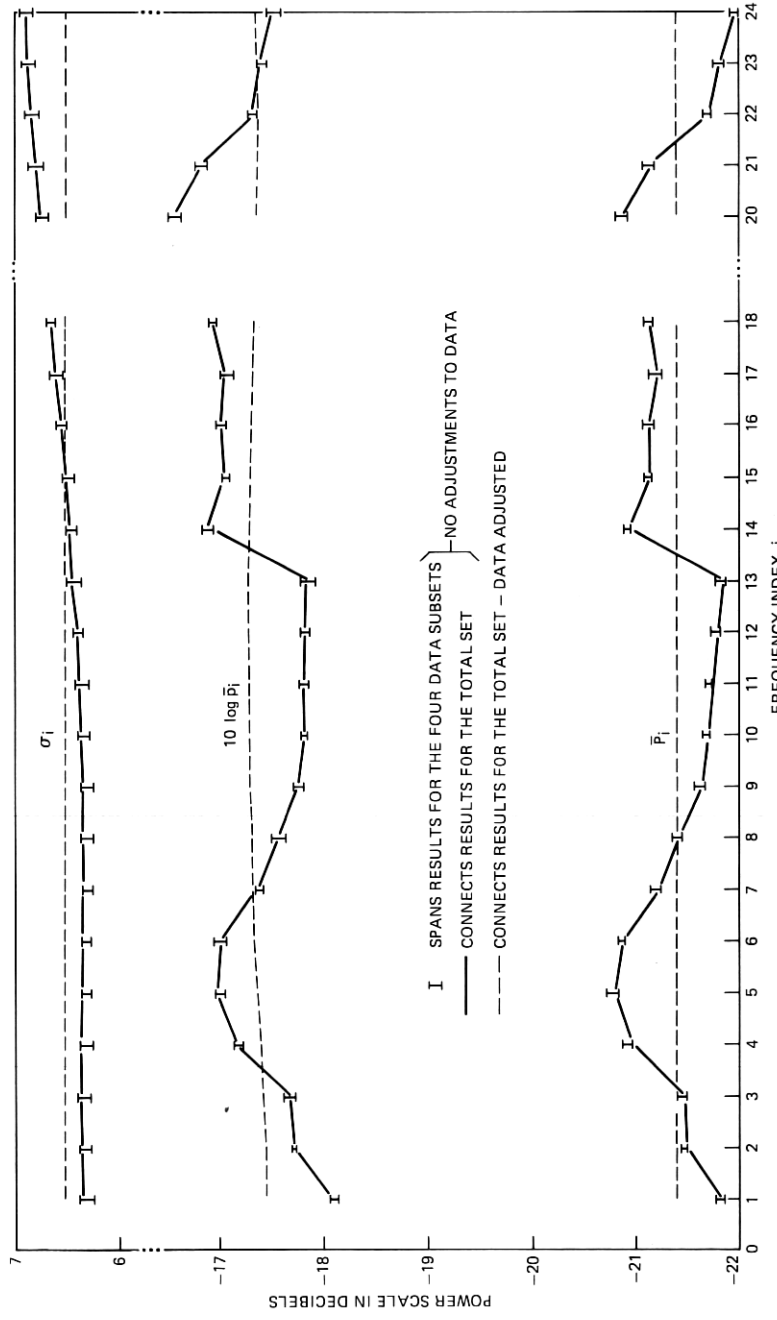

Fig. 2—Moments of the recorded power gains, as functions of frequency, before and after data adjustments.

effects, and to compensate for them using simple adjustments of all the P_i's in the data base. The adjustments are of the form

$$P_i \Rightarrow \alpha_i P_i + \beta_i; \quad \text{each } i, \tag{19}$$

where the variations of α_i and β_i with i are chosen to serve two purposes. One is to render the ensemble means and variances of the adjusted P_i's uniform over i. The other is to conserve the "'global" mean and variance ($\bar{P}$ and σ^2) of P_i, i.e., the mean and variance of the P_i's taken over the entire data base (24,820 records × 23 samples/record). It is easy to show that this is achieved by choosing α_i and β_i as

$$\alpha_i = \frac{\sigma}{\sigma_i}, \quad \beta_i = \bar{P} - \frac{\sigma}{\sigma_i}\bar{P}_i; \quad \text{each } i. \tag{20}$$

The variations of $\bar{P}_i$, σ_i, and 10 log $\bar{p}_i$ for the entire record set, when the data are adjusted according to (19) and (20), are given in Fig. 2 by the dashed curves. We see that, by making $\bar{P}_i$ and σ_i uniform over i, 10 log $\bar{p}_i$ has been made nearly uniform also, as we expect it to be from physical considerations. The α_i's and β_i's that produce these results are close to 1.0 and 0.0 dB, respectively, for all i.*

Though minor, the data adjustments have measurably reduced the curve-fitting errors associated with the next stage of reduction. This is made evident later.

4.2.2 Coefficients of the power gain polynomial

4.2.2.1 Least Squares Method. We wish to compute, for given M, those D_m's in eq. (3) that yield the best approximation to the channel power response in each record. Ideally, we would like to minimize some measure of $(Q_i - R_i)$ (see Table I), such as its mean-square average over i, $\langle \epsilon_i^2 \rangle$. Since the values of R_i are unknowable, the next best thing is to minimize some measure of $(P_i - Q_i)$, such as $\langle E_i^2 \rangle \equiv E_{\text{rms}}^2$. However, the Q_i's are logarithms of samples of $q(\omega)$, and so a precise least-squares minimization is not analytically tractable. Fortunately, so long as $|E_i| < 1$ dB for most i, E_{rms}^2 can be accurately approximated by $\hat{E}_{\text{rms}}^2$, as given in Table I. This quantity lends itself to least-squares minimization.

For a given M and a given record, the following approach is used to find $D_0, \cdots D_M$: (*i*) the 23 P_i's are converted to power ratios, p_i; (*ii*) the function $\hat{E}_{\text{rms}}^2$ is expressed in terms of the D_m's in eq. (3); (*iii*) the $M + 1$ derivatives of $\hat{E}_{\text{rms}}^2$ with respect to $D_0, \cdots D_M$ are computed and equated to zero; and (*iv*) the resulting $M + 1$ linear equations in $D_0, \cdots D_M$ are solved using matrix methods.

---

* The α_i's range from 0.945 to 1.029, and the β_i's range from −0.99 dB to 1.25 dB.

As a refinement to this procedure, we add one more step: The derived D_m's are multiplied by a common factor chosen to force the bias error, $\langle E_i \rangle \equiv E_B$, to zero.* Thus, for example, if the initial solution for the D_m's leads to a bias error $E_B = X$, then adjusting each D_m by a multiplying factor $10^{X/10}$ will reduce E_B to zero. This step reduces E_{rms} and makes the Q_i's unbiased estimators of the P_i's.

Figure 3 shows two sample records for P_i, taken from the data base. In each case, the function $Q(\omega) = 10 \log q(\omega)$, as computed using the above procedure, is plotted for $M = 0$, 2, and 4. Note that, for $M = 0$, the fitting function lacks the curvature needed to accommodate typical fading patterns. For $M = 4$, on the other hand, the fitting function provides added curvature that may be artificial, i.e., it may serve to fit the measurement noise more than the underlying response. We now turn to a discussion of fitting errors and the most suitable choice for M.

4.2.2.2 Random Error Model. To begin, assume that 23 noisy samples of P_i are to be fitted by $Q(\omega) = 10 \log q(\omega)$. Assume, further, that the sample errors $e_i = (P_i - R_i)$ are independent, zero-mean Gaussian variables, each having an rms value σ_{meas}. Since the R_i's are unknowable, the e_i's cannot be observed directly; at best, their statistics can be inferred from an analysis of the observed errors, $E_i = P_i - Q_i$.

Specifically, suppose that M is a sufficiently high polynomial order that, in the absence of measurement noise, all significant variations of P_i with i could be accommodated by the fitting function $Q(\omega)$. In that case, all the E_i's would be due solely to measurement errors, the e_i's. To a first approximation, we could then say the following:[8] The E_i's are zero-mean Gaussian variables, each having an ensemble mean-square value

$$\overline{E_i^2} = \frac{22 - M}{23} \sigma_{\text{meas}}^2; \quad \text{each } i. \tag{21}$$

In addition, E_{rms}^2 is chi-square distributed, with $22 - M$ degrees of freedom and a mean given by eq. (21), i.e., $\overline{E_{\text{rms}}^2} = \overline{E_i^2}$. Finally, the errors of major interest, $\epsilon_i = (Q_i - R_i)$, are zero-mean Gaussian variables, each having a mean square value

$$\epsilon_i^2 \equiv \sigma_\epsilon^2 = \overline{e_i^2} - \overline{E_i^2}$$

$$= \frac{M + 1}{23} \sigma_{\text{meas}}^2; \quad \text{each } i. \tag{22}$$

The pertinence of this theory to our data reductions is as follows: If the observed E_i's are essentially zero-mean and Gauss-distributed

* Remember that the least-squares method is applied to $\hat{E}_{\text{rms}}^2$ rather than to the quantity of interest, E_{rms}^2. The possibility thus exists of a small bias error in the results, which this step removes.

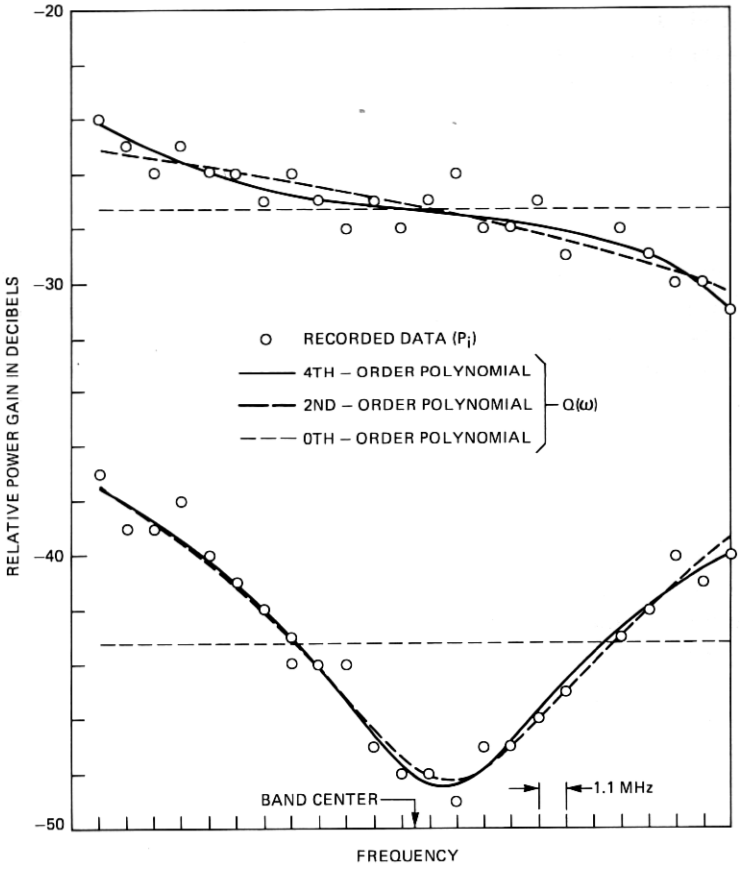

Fig. 3—Two examples of data records and their representations by zeroth-, second-, and fourth-order polynomials.

across the data ensemble, each with the same $\overline{E_i^2}$; and if E_{rms}^2 is chi-square distributed with $22 - M$ degrees of freedom and a mean of $\overline{E_i^2}$, then the random-error model, as described above, can be assumed to apply. Accordingly, σ_{meas}^2 can then be estimated from measured error statistics using eq. (21), and the mean-square error between the fitted and true power gains can be estimated using eq. (22).

The reduced data show that, when $M = 0$, the populations of E_{rms}^2 and the E_i's do not have the properties of the random error model. This is to be expected, since a zeroth-order polynomial (horizontal line) cannot accommodate the true variations of faded power with frequency; hence, the E_i's are caused mostly by the inadequacy of the fitting function rather than by measurement noise.

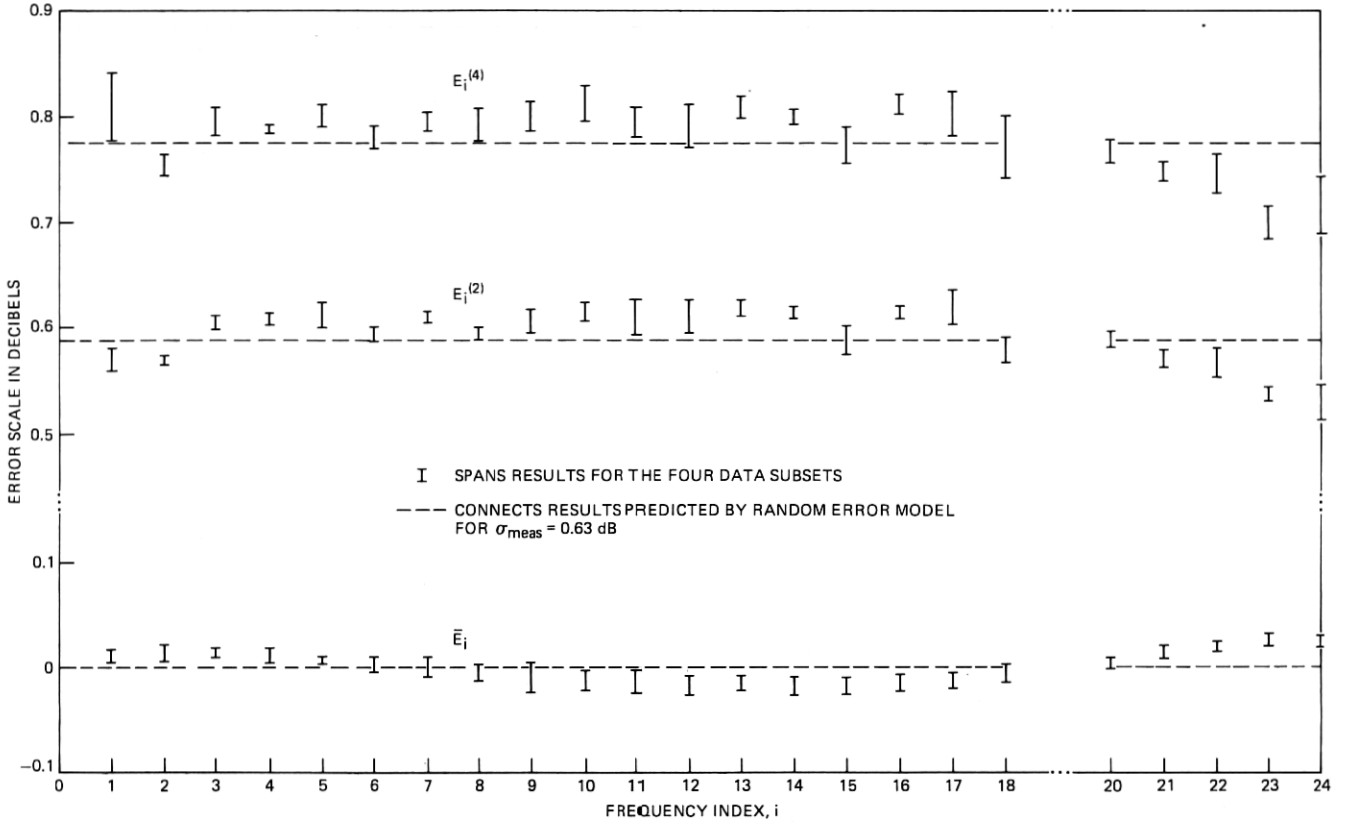

Fig. 4—Moments of observed fitting errors for $M = 2$, as functions of frequency, compared with values predicted by the random error model.

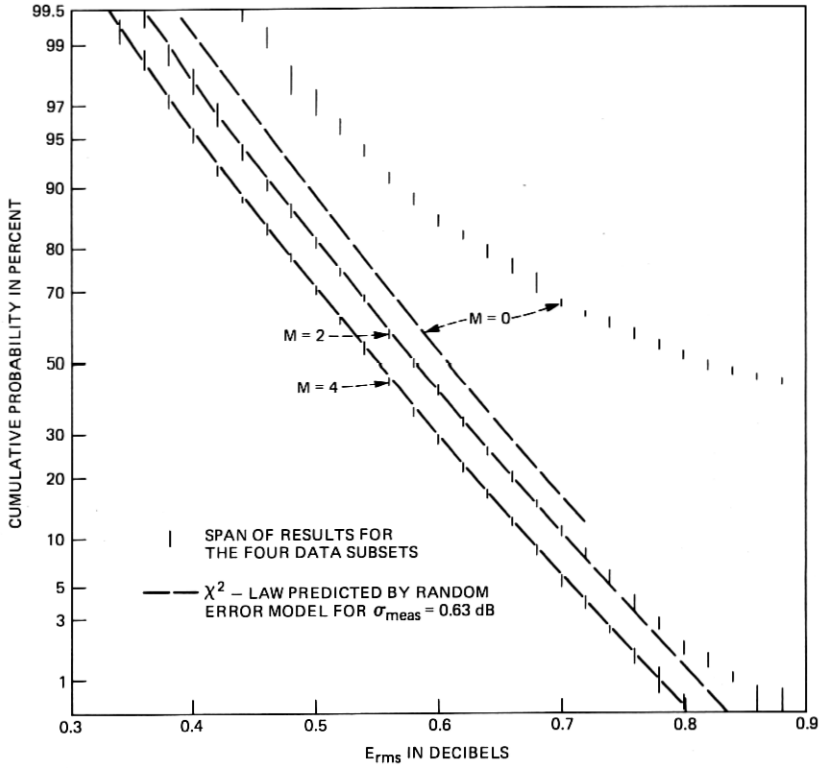

Fig. 5—Probability distributions for E_{rms}, using zeroth-, second-, and fourth-order polynomials, compared with chi-square distributions predicted by the random-error model.

For $M = 2$ and $M = 4$, however, the populations of E_{rms}^2 and the E_i's do exhibit the properties of the random error model. For example, Fig. 4 shows variations of $\overline{E_i}$, $E_i^{(2)}$ and $E_i^{(4)}$ with i for $M = 2$ (see Table I). Each vertical bar spans the spread of values among the four data subsets, while the dashed lines give the values predicted by the random error model.

Figure 5 gives even stronger evidence for the random error model when $M \geq 2$. The vertical axis represents $\Pr\{E_{rms} > \text{abscissa}\}$, the vertical bars give the spread of this quantity among the four data subsets, and the dashed curves give the variations predicted by the random error model when $\sigma_{meas} = 0.63$ dB. For $M = 0$, the measured results compare very poorly with the predictions, for the reasons noted above, while for $M = 2$ and $M = 4$ they compare very well. Using eq. (22), the errors between Q_i and R_i are found to have the rms values $\sigma_\epsilon = 0.23$ dB for $M = 2$ and $\sigma_\epsilon = 0.29$ dB for $M = 4$.

The rms modeling error, σ_ϵ, is smaller for $M = 2$ because only three polynomial coefficients are derived from 23 recorded samples, leaving 20 degrees of freedom for averaging out measurement noise. For $M = 4$, five polynomial coefficients are derived, leaving 18 degrees of freedom for noise averaging. We conclude that, for modeling purposes, M should be large enough to provide adequate curvature in $q(\omega)$ (as evidenced by E_i- and E^2_{rms}-populations that fit the random error model), but no larger (so as to minimize σ_ϵ). In view of this criterion, we have decided that $M = 2$ is the optimal polynomial order for the present data base.

Table II gives computed ensemble averages for $\hat{E}^2_{\text{rms}}$ (the statistic minimized by least-squares methods) and E^2_{rms} for $M = 0$, 2, and 4. The ensemble in this case was the four merged data subsets. The close agreements between $\overline{\hat{E}^2_{\text{rms}}}$ and $\overline{E^2_{\text{rms}}}$ for both values of M justify the approximation of E^2_{rms} by $\hat{E}^2_{\text{rms}}$ in the least-squares derivation of the D_m's.

The results in Table II also permit comparisons between the cases where the recorded data are adjusted, as described in Section 4.2.1, and not adjusted. The reduction in fitting error associated with these adjustments is small but distinct, indicating that the inferred calibration differences are real.

4.2.2.3 Coefficient Distributions. We have determined (D_0, D_1, D_2) for every record in the total set, using the least-squares fitting procedure described above. This effort has led to the set of cumulative probability distributions in Figs. 6, 7, and 8. In each case, the vertical bars span the results for the four data subsets, while the solid curve gives the result for the total set. In some cases, where the probability curve is steep and the spreads are small, the vertical bars can barely be distinguished. In all three figures, the results show good consistency among the four subsets and the total set.

The distribution for D_0, Fig. 6, is worth special note. From eq. (3), it is clear that D_0 can be interpreted as the power-gain ratio at the center of the channel ($\omega = 0$). Accordingly, it must always be positive, whereas D_1 and D_2 can have either polarity. Also, since the power-gain statistics should be the same at each frequency, the decibel value of D_0 should have the same distribution as do the P_i's. For that reason, the abscissa

Table II—Error statistics for 8640 records

Measured Error Statistics	$M = 0$		$M = 2$		$M = 4$	
	Data Adjusted	No Adjustment	Data Adjusted	No Adjustment	Data Adjusted	No Adjustment
$\overline{\hat{E}^2_{\text{rms}}}$ in dB^2	—	—	0.361	0.486	0.314	0.373
$\overline{E^2_{\text{rms}}}$ in dB^2	1.698	1.880	0.351	0.473	0.311	0.368

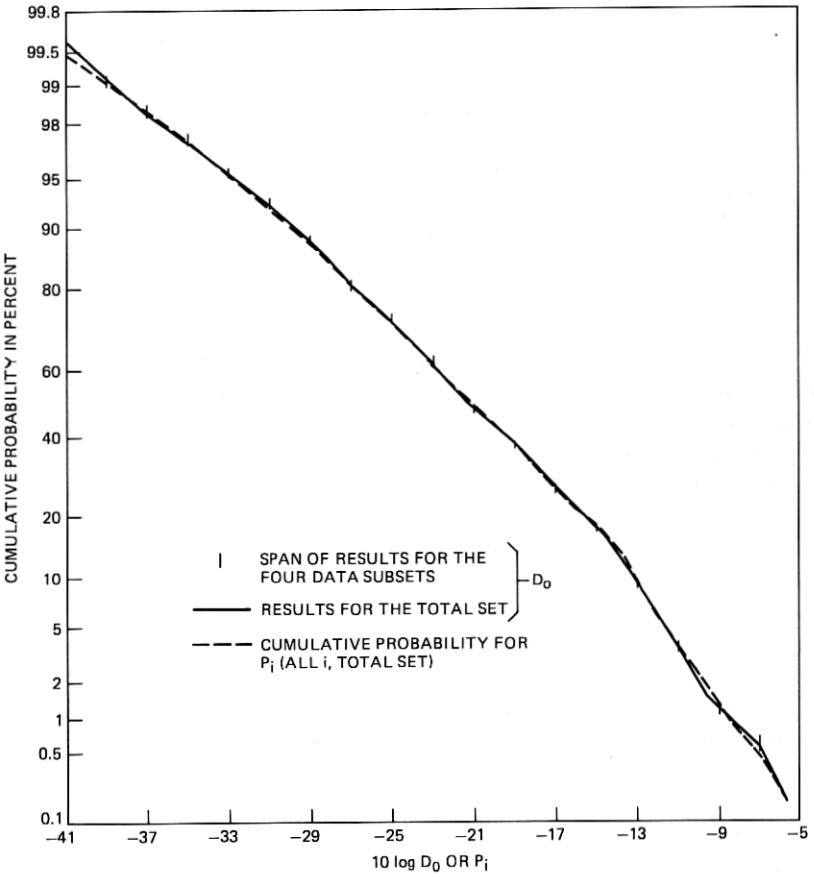

Fig. 6—Probability distributions for power-gain polynomial coefficient D_0 and recorded, adjusted dB power-gain P_i.

in Fig. 6 is scaled in units of 10 log D_0, and the distribution for all P_i's in the data base (24,820 records × 23 samples/record) is given as well (dashed curve). The agreement between the dashed and solid curves is excellent, as we should expect.

It should also be noted that a straight line on the probability paper used here would imply a Gaussian (or normal) probability law. Thus, 10 log D_0 is nearly normal, i.e., D_0 is approximately log-normal. Since $A_0 = \sqrt{D_0}$ (eq. (7a)), this means that A_0 is also approximately log-normal, as we have noted in Section III.

4.2.3 Coefficients of the complex gain polynomial

The method for computing the A_n's and B_n's from the D_m's for $M = 2$ was outlined in Section 2.2. The primary results are given by eqs. (6) and (7). The condition $\Delta \geq 0$ occurs over 58 percent of the data

records, in which cases $|H_c(\omega)|^2$ can be matched to $q(\omega)$ without requiring a second-order coefficient (i.e., $A_2 = B_2 = 0$). Over the 42 percent of the records wherein $\Delta < 0$, however, $A_2, B_2 \neq 0$, and a small but nonzero fourth-order term, $(A_2^2 + B_2^2)\omega^4$, exists in $|H_c(\omega)|^2$. Although the method of solution is designed to minimize this term, it is necessary to evaluate its effect on the polynomial fitting.

We define the added distortion, δ, for a given record to be the rms decibel difference between $|H_c(\omega)|^2$ and $q(\omega)$, where the rms averaging is over i. Thus,

$$\delta = \sqrt{\langle 10 \log \left\{ \frac{q(\omega_i) + (A_2^2 + B_2^2)\omega_i^4}{q(\omega_i)} \right\} \rangle}. \tag{23}$$

Clearly, $\delta = 0$ for records in which $\Delta \geq 0$. We have computed a cumulative distribution for nonzero δ over 3600 records, specifically,

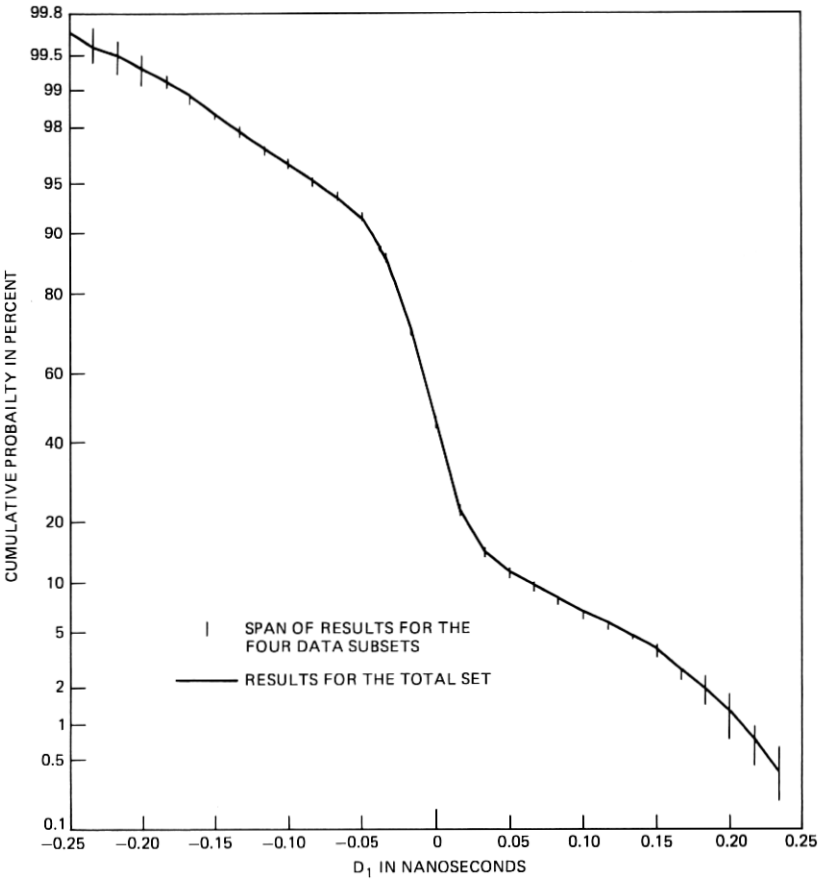

Fig. 7—Probability distribution for power-gain polynomial coefficient D_1.

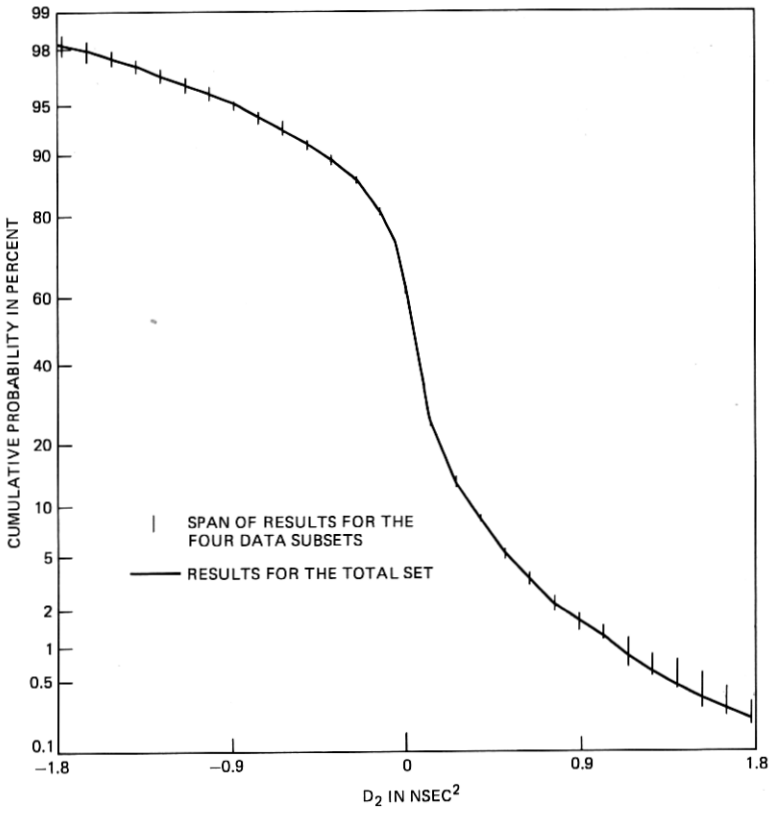

Fig. 8—Probability distribution for power-gain polynomial coefficient D_2.

those records within the four merged subsets where $\Delta < 0$. The result (Fig. 9) is that, for 99.4 percent of these records, δ is below 0.23 dB, i.e., smaller than the rms error due to noise. Over all records, moreover, δ is less than 0.52 dB.

Having established the accuracy of the procedure for computing the A_n's and B_n's, we have elected to ignore those nonzero values of A_2 and B_2 that arise in 42 percent of the records. This step permits a simpler model, as noted previously, at some cost in accuracy. Justification for it is given in Section V.

4.3 Deriving the coefficient statistics

Assume now that the set (A_0, A_1, B_1) is derived, record by record, for the total data base. Using this large population of coefficient sets, it should be possible to obtain a mathematical description for the pdf $p(A_0, A_1, B_1)$. The procedure used was outlined in Section 2.3, and the result was presented in Section III. In the following discussion, we

present the evidence for (*i*) the pdf of a_o [eqs. (14) to (16)]; (*ii*) the pdf's of A_1 and B_1 conditioned on a_o; (*iii*) the functional variations of σ_A and σ_B with a_o [eqs. (17) and (18)]; and (*iv*) the statistical independence of A_1 and B_1 for given a_o.

4.3.1 PDF for a_o

The quantity a_o is a shifted, scaled version of 20 log A_0 which, from eq. (7a), is identical to 10 log D_0. The empirical distribution for this variate in Fig. 6 is represented in Fig. 10 by the circles. The dashed curve in Fig. 10 is based upon the pdf for a_o given by eqs. (15) and (16). We conclude, then, that our mathematical model for the distribution of 20 log A_0 is an accurate one.

4.3.2 Conditional PDF's for A_1 and B_1

To derive the pdf's of A_1 and B_1, conditioned on a_o, the 24,820 data records were grouped into 11 subpopulations, each corresponding to a particular range of a_o. For each of the central nine subpopulations, the a_o-range has a width of one-half a standard deviation, thereby balancing the objectives of good resolution (narrow a_o-range per subpopulation) and sample size sufficiency (many records per subpopulation).

Within each subpopulation, we computed the mean, standard deviation and cumulative distribution for A_1, and similarly for B_1. Since the

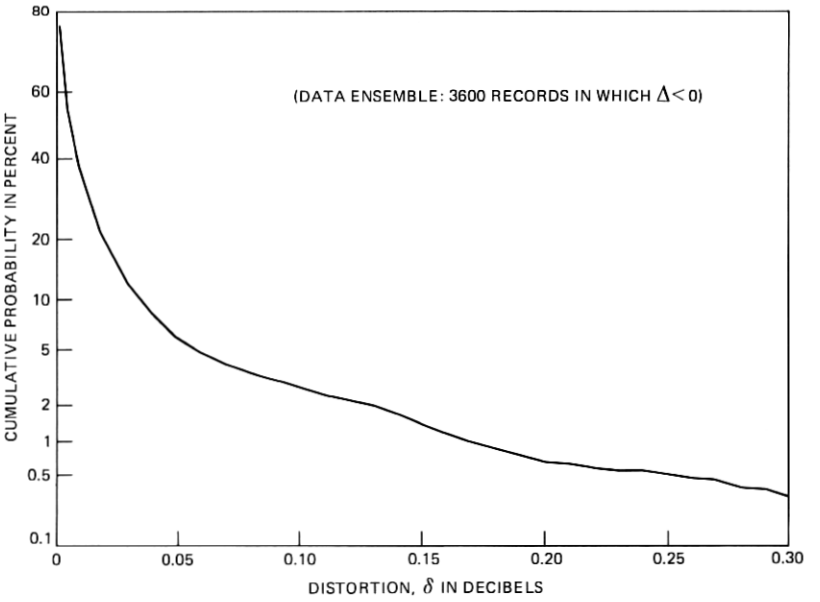

Fig. 9—Probability distribution for distortion term δ, caused by nonzero fourth-order coefficient in records for which $\Delta < 0$.

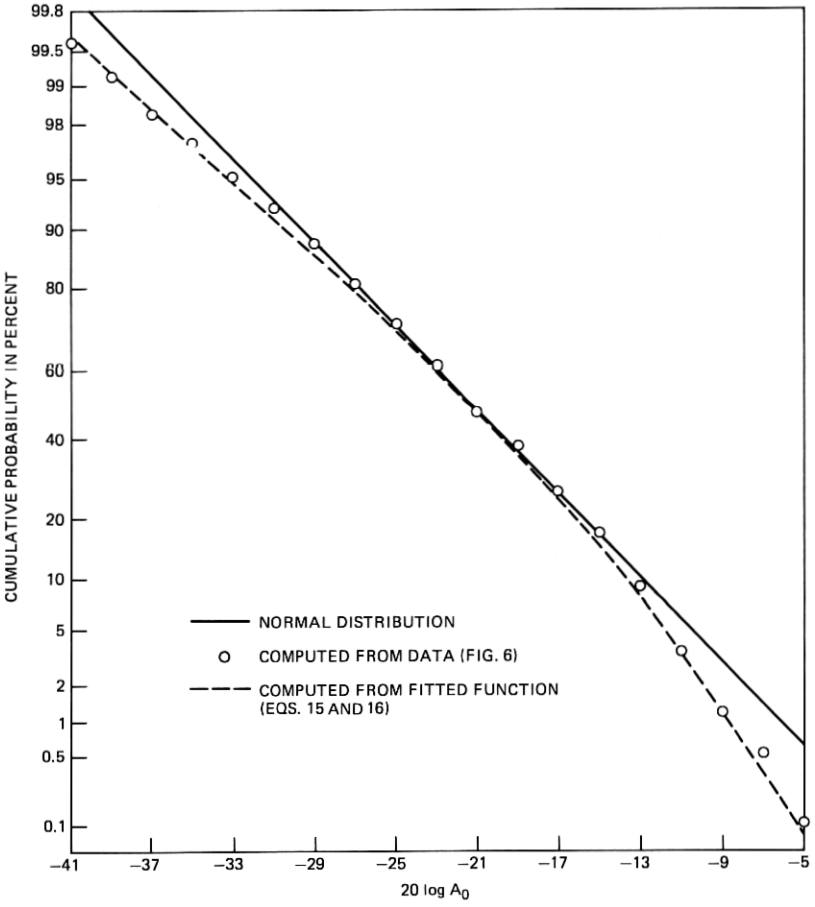

Fig. 10—Probability distributions (empirical and mathematical model) for complex gain polynomial coefficient A_0.

polarity of A_1 was chosen randomly in each data record (a reaction to the absence of phase response data, as noted in Section 2.2), the mean for A_1 was very close to zero in every subpopulation.

We also randomized the polarity of every reduced value of B_1 before analyzing the B_1 statistics in each subpopulation. The motive for this polarity randomization is that it simplifies the statistical modeling. Before randomization, the conditional mean of B_1 was not close to zero in every subpopulation, nor was its conditional distribution Gauss-like; *after* randomization, B_1 became a zero-mean Gauss-like variable in every subpopulation. Although this simplification entailed some doctoring of the derived B_1's, it should be noted that the polarity of B_1 is immaterial in any practical system context. For this quantity repre-

sents the slope, at band center, of the real part of $H_c(\omega)$, and whether the slope is upward to the right (B_1 negative) or upward to the left (B_1 positive) has no effect on either detection behavior or the realizability of equalizer circuits. The same cannot be said for the polarity of A_1, which can influence the stability of some equalizer designs.

Table III gives some pertinent data for the 11 subpopulations analyzed. For each one, identified by a number and an a_o-range, the table gives the number of records contained therein and the standard deviations for A_1 and B_1. Because of the polarity randomizations, the means for A_1 and B_1 are essentially zero in every case.

Some distributions for A_1/σ_A and B_1/σ_B are indicated in Figs. 11 and 12, respectively. Data are given for only five of the subpopulations, but all of the nine central subpopulations exhibit the Gauss-like distributions evident here. That is, A_1/σ_A and B_1/σ_B act, in every case, like zero-mean, unit-variance Gaussian variables. We can therefore invoke the following models:

$$p_A(A_1 \mid a_o) = \frac{1}{\sqrt{2\pi}\,\sigma_A(a_o)} \exp\left\{ -\frac{1}{2}\frac{A_1^2}{\sigma_A^2(a_o)} \right\} \tag{24}$$

and

$$p_B(B_1 \mid a_o) = \frac{1}{\sqrt{2\pi}\,\sigma_B(a_o)} \exp\left\{ -\frac{1}{2}\frac{B_1^2}{\sigma_B^2(a_o)} \right\}. \tag{25}$$

4.3.3 $\sigma_A(a_o)$ and $\sigma_B(a_o)$

Let us associate each σ_A in Table III with the midvalue of the a_o-range for which it is computed and do the same for each σ_B. (This procedure has no meaning, of course, for the semi-infinite ranges of the first and last subpopulations.) The result is that the circles and crosses in Fig. 13 can be regarded as samples of the functions $\sigma_A(a_o)$ and $\sigma_B(a_o)$, respectively. The solid curves provide accurate fits to these data that are described mathematically by eqs. (17) and (18).

Table III—Data for the 11 subpopulations

Subpop. Number	a_o-Interval	Population Size	σ_A (ns)	σ_B (ns)
1	< -2.25	515	0.154	0.126
2	$[-2.25, 1.75)$	660	0.153	0.125
3	$[-1.75, -1.25)$	1423	0.141	0.121
4	$[-1.25, -0.75)$	2878	0.176	0.140
5	$[-0.75, -0.25)$	4147	0.240	0.186
6	$[-0.25, 0.25]$	4925	0.278	0.175
7	$(0.25, 0.75]$	4340	0.370	0.185
8	$(0.75, 1.25]$	3522	0.440	0.239
9	$(1.25, 1.75]$	1933	0.503	0.233
10	$(1.75, 2.25]$	371	0.576	0.218
11	>2.25	106	0.656	0.158
		Total: 24,820		

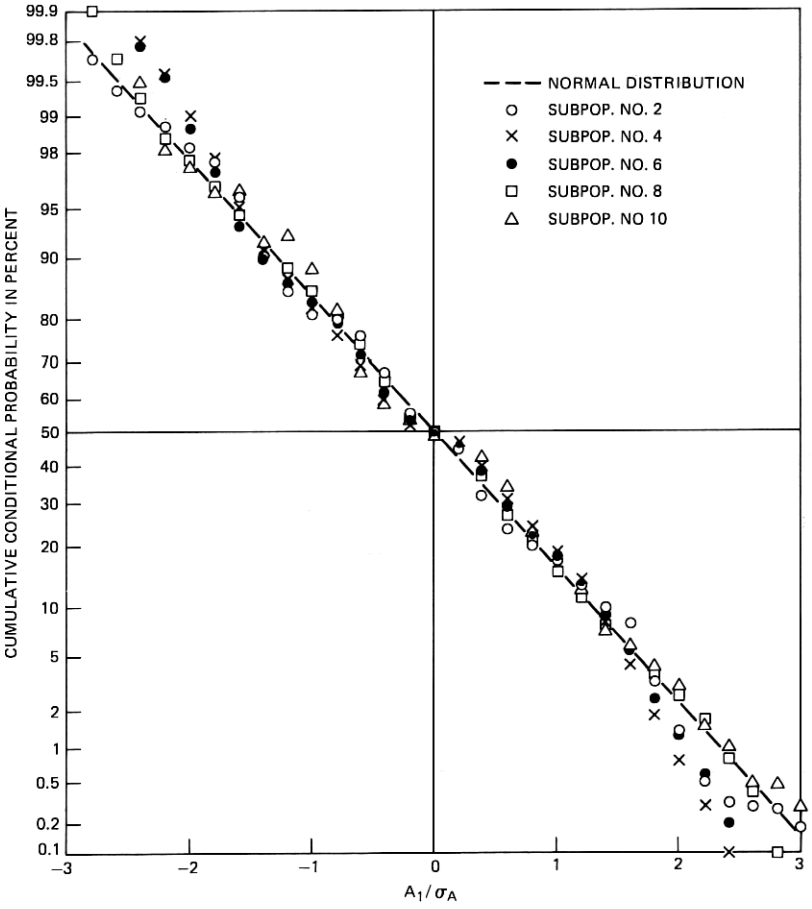

Fig. 11—Probability distributions for A_1/σ_A, conditioned on a_o, for five subpopulations.

4.3.4 Statistical independence of A_1 and B_1

Formal statistical testing has shown that A_1 and B_1 within each subpopulation are *not* mutually independent. We have assumed such independence anyway because of the resulting simplification of the model. The validity of this approach rests upon how it influences the outcome of system studies. The next section takes up this issue and gives justification for treating A_1 and B_1, conditioned as a_o, as independent variables.

V. ACCURACY OF THE MODEL

The multipath fading model presented here consists of (*i*) a polynomial representation for $H_c(\omega)$; (*ii*) a mathematical formula for the

joint coefficient pdf; and (*iii*) a formula for T_M, the number of fading seconds per heavy-fading month. We now discuss the accuracy of each of these constituents.

5.1 The polynomial representation

The first step in using the polynomial representation consists of fitting $q(\omega)$, eq. (3), to the recorded power gain data. This was done, with $M = 2$, for each of 24,820 records. The error measured in each record is the rms decibel difference (E_{rms}) between the recorded and fitted power gains. Although the error between $q(\omega)$ and the true underlying response cannot be estimated from isolated records, its statistics can be inferred by analyzing the population of E_{rms} over

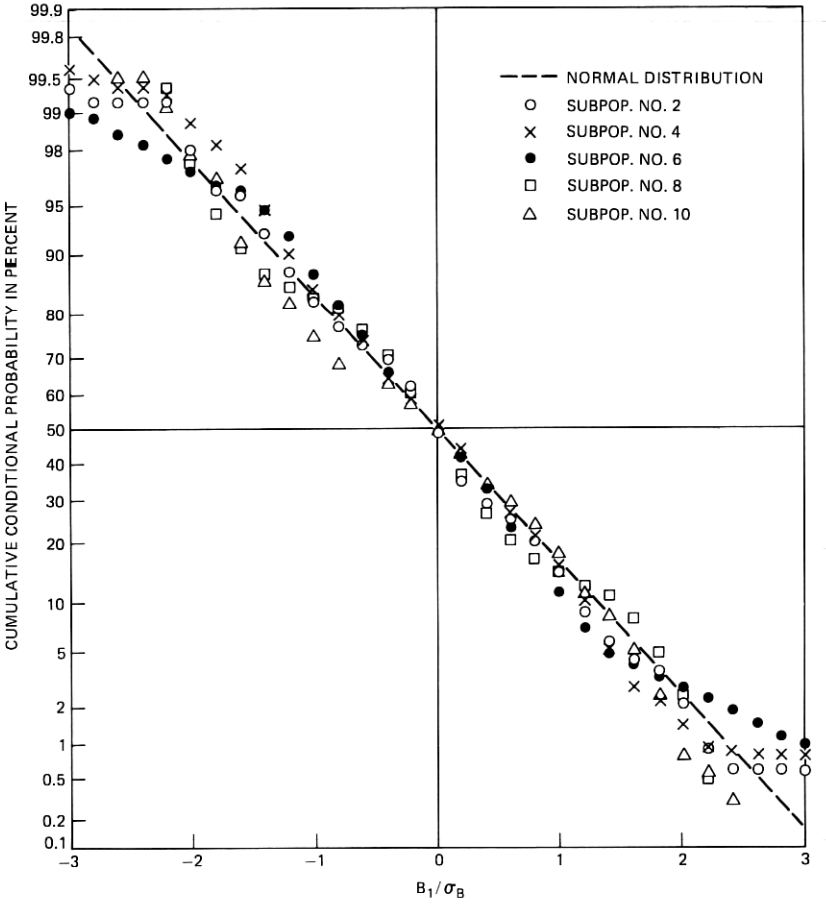

Fig. 12—Probability distributions for B_1/σ_B, conditioned on a_o, for five subpopulations.

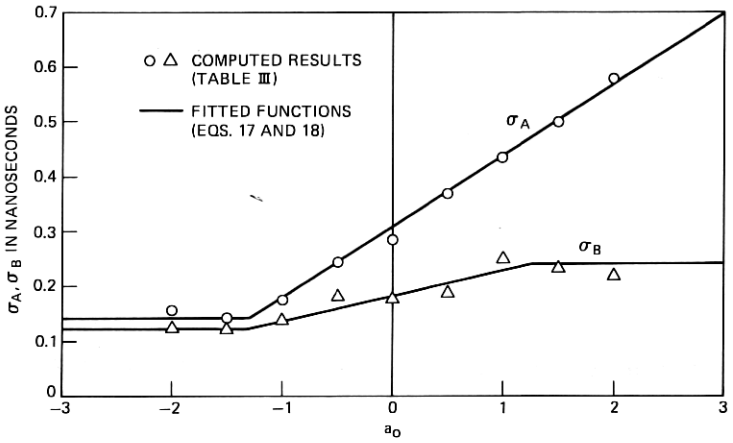

Fig. 13—Variations (empirical and mathematical model) of σ_A and σ_B with a_o.

thousands of records. Such an analysis* had led to the following conclusion: The decibel difference between the fitted and true power gains is approximately Gauss-distributed at each frequency, is due almost entirely to measurement noise (rather than inadequate curvature in the form of $q(\omega)$), and has an rms value of 0.23 dB. This corresponds to an rms error of 2.7 percent in the gain magnitude, $|H_c|$, which is sufficiently low for purposes of modeling.

The next step in the polynomial representation is to derive the A- and B-coefficients in eq. (2) from the D-coefficients in eq. (3). For 58 percent of the data records, coefficient sets (A_0, A_1, B_1) exist which provide a perfect match between $|H_c(\omega)|^2$ and $q(\omega)$. The one flaw in these cases is the unresolvable ambiguity (resulting from noncoherent measurements) in the polarity of A_1.

For the remaining 42 percent of the records, the method for choosing A's and B's leads, in addition, to nonzero A_2 and B_2 and a resulting fourth-order term in $|H_c(\omega)|^2$ not present in $q(\omega)$. The differences between $|H_c(\omega)|^2$ and $q(\omega)$ for these records were analyzed, and found to be minor (see Section 4.2.3 for more details).

Finally, all nonzero values computed for A_2 and B_2 have been discarded to simplify the model. To evaluate the validity of this step, we performed an outage analysis for several different modulations, specifically, 4-PSK, 8-PSK, 16-PSK and 16-QAM. For each modulation, cosine rolloff spectral shaping was assumed, and the rolloff factor (α) and channel bandwidth (W) were treated as variables. In every case,

* It is noteworthy that the distribution for E^2_{rms} derived here using a second-order $q(\omega)$ is nearly identical to that obtained for the three-path model of Rummler (Ref. 5). The slightly lower mean obtained here is due solely to the data adjustments described in Section IV.

we specified the symbol rate to be $W/(1 + \alpha)$, thereby matching the truncation bandwidth of the modulation to the channel bandwidth.

The outage analysis performed for each modulation used $W = 20$, 30, and 40 MHz and α-values between 0.1 and 1.0. For each of the resulting cases, the quantity "outage seconds/heavy-fading month" was estimated using the following procedure: Regions of the coefficient set $(A_0, A_1, B_1, A_2, B_2)$ for which the detected data eye is closed were derived analytically;* the number of data records for which $(A_0, \cdots B_2)$ lies within these so-called outage regions was counted; and the fraction of these records was multiplied by T_M in eq. (12). [We assumed $c = 1$ (average terrain), $F = 6$ (GHz), and $d = 26.4$ (miles), resulting in a value for T_M of 12,144 s].

This computation was done twice for each combination of modulation, W and α. In one computation, nonzero values of A_2 and B_2 were acknowledged in comparing each $(A_0, \cdots B_2)$ to the outage regions; in the other, A_2 and B_2 in each record were taken to be zero.

The numerical results span a range from 5 to 8000 seconds of outage. The results obtained by acknowledging nonzero (A_2, B_2) pairs and the results obtained by ignoring them differ by less than 10 percent for all cases treated. The simplification of omitting A_2 and B_2 from the model is thus found to be acceptable for purposes of making outage predictions.

5.2 The coefficient PDF

In deriving the mathematical result for $p(a_o, A_1, B_1)$, Section III, numerous approximations and assumptions were made, e.g., independence between A_1 and B_1 for given a_o; Gaussian conditional pdf's for A_1 and B_1; and the functions for $p_a(a_o)$, $\sigma_A(a_o)$, and $\sigma_B(a_o)$. The ultimate test of the result is whether it leads to the same performance predictions as those based upon the actual population of coefficient sets. Accordingly, outage seconds for the combinations of modulation, W, and α cited above were obtained using a separate method of calculation: In addition to counting data records over the coefficient outage regions, the model distribution $p(a_o, A_1, B_1)$ was integrated over these regions.

The main findings are as follows: When the outage calculated by counting data records is greater than 70 seconds per heavy-fading month, the outage calculated by integrating $p(a_o, A_1, B_1)$ differs by 16 percent or less; for outages less than 70 seconds, the difference is 50 percent or less. This is an excellent level of agreement for practical purposes.

---

* The closed-eye criterion for "outage" leads to conservative performance measures but has the virtue of not depending on system fade margin or specified bit error rate; it also simplifies the outage analysis considerably.

The above findings vindicate the modeling assumption that A_1 and B_1 are independent for given a_o. It also confirms the accuracy of the functions used for $p_a(a_o)$, $\sigma_A(a_o)$, and $\sigma_B(a_o)$. It is noteworthy that, when outage is calculated using a purely Gaussian function for $p_a(a_o)$ [i.e., $z(a_o) = 0$ in eq. (16)], the agreement with counted data records is poor in several cases. In short, the refinement in $p_a(a_o)$ used here is important to the accurate use of the model in system outage predictions.

5.3 Expression for T_M

The expression given for T_M in Section III assumes only that this quantity is in a fixed proportion to the multipath occurrence factor of Barnett.[7] By computing the fading time and occurrence factor for the present data base, we have obtained the empirical results of eq. (12). This result is unverified, although recent studies have indicated that it is reliable to within a factor or two.[9]

There is further evidence supporting eq. (12) for T_M, as well as eq. (1) for $p_a(a_o)$: Using these two formulas, plus (14) and (16), we can show that deep fades observe the probability law

$$\Pr\{A_0 < L\} \doteq 1.7\, rL^2; \quad (-10 \log L^2 > 26 \text{ dB}). \tag{26}$$

This law applies to heavy-fading months, and r is the multipath occurrence factor used to derive T_M. This result differs from that of Barnett[7] by the factor 1.7, which represents very good agreement.

VI. DISCUSSION AND CONCLUSION

We have presented a statistical model for describing the microwave channel distortions classified as multipath fading. The model is defined by the functions of eqs. (11) through (18) and by the 12 numerical constants contained therein. We do not know whether the functional structure is valid for other paths, microwave frequencies, seasons, etc., and, if it is, whether or how the numerical constants vary with these conditions. The way to resolve these questions is through more multipath experiments.

A major virtue of the polynomial model suggested by eq. (2) is the simplicity it affords in analyzing the response of a fading channel to arbitrary modulations. This is largely because the required polynomial order for $H_c(\omega)$ in channelized microwave systems is generally quite low. Ample support for this conclusion is given by the data reductions and system analysis results reported here.

Another useful feature of the polynomial model is that it suggests the form of an adaptive equalizer response, i.e., $1/H_c(\omega)$, which is easy to realize when the complex zeros of $H_c(\omega)$ have negative real parts. With this in mind, the polarity of A_1 becomes a very important

issue. For when $A_1 > 0$, the realizable adaptive response $[A_o - \omega B_1 + j\omega |A_1|]^{-1}$ is highly effective against multipath fading.[10] When $A_1 < 0$, however, such a response eliminates amplitude distortion at the cost of increased delay distortion. In lieu of explicative data, the present model assumes that $A_1 < 0$ precisely half the time. Whether this is true or not has important bearing on the achievement of successful equalizer approaches. Coherent multipath measurements would help to resolve the existing polarity uncertainty in the model.

The new model provides a useful starting point for the design of subsequent experiments. What it reveals about the depth, shape, and statistics of multipath fading responses can facilitate design choices for the channel probing signal, receiver processing, data acquisition and reduction strategies, and other experiment features.

REFERENCES

1. C. W. Anderson, S. Barber and R. Patel, "The Effect of Selective Fading on Digital Radio," Paper No. 33.5, ICC Conf. Record, June 1978.
2. L. J. Greenstein and V. K. Prabhu, "Analysis of Multipath Outage with Applications to 90-Mb/s PSK Systems at 6 and 11 GHz," IEEE Trans. Commun., *COM-27*, No. 1 (January 1979), pp. 68–75.
3. W. C. Jakes, Jr., "An Approximate Method to Estimate an Upper Bound on the Effect of Multipath Delay Distortion on Digital Transmission," IEEE Trans. on Comm., *COM-27*, No. 1 (January 1979), pp. 76–81.
4. C. W. Lundgren and W. D. Rummler, "Digital Radio Outage Due to Selective Fading—Observation vs. Prediction from Laboratory Simulation," B.S.T.J., *58*, No. 5 (May–June 1979), pp. 1073–1100.
5. W. D. Rummler, "A New Selective Fading Model: Application to Propagation Data," B.S.T.J., *58*, No. 5 (May–June 1979), pp. 1037–1071.
6. L. J. Greenstein, "A Multipath Fading Channel Model for Terrestrial Digital Radio Systems," IEEE Trans. on Commun., *COM-26*, No. 8 (August 1978), pp. 1247–1250.
7. W. T. Barnett, "Multipath Propagation at 4, 6 and 11 GHz," B.S.T.J., *51*, No. 2 (February 1972), pp. 321–361.
8. J. R. Green and D. Margerison, *Statistical Treatment of Experimental Data*, Elsevier, 1977; Chs 13 and 15.
9. W. D. Rummler, "Extensions of the Multipath Fading Channel Model," Paper No. 32.2, ICC Conf. Record, June 1979.
10. L. J. Greenstein and D. Vitello, "Digital Radio Receiver Responses for Combating Frequency-Selective Fading," IEEE Trans. on Commun., *COM-27*, No. 4 (April 1979), pp. 671–681.